

Real-fluid behavior in rapid compression machines: Does it matter?

Mingrui Wang^a, S. Scott Goldsborough^b, Song Cheng^{a,c*}

^a*Department of Mechanical Engineering, The Hong Kong Polytechnic University, Kowloon, Hong Kong SAR, China*

^b*Transportation and Power Systems Division, Argonne National Laboratory, Lemont, USA*

^c*Research Institute for Smart Energy, The Hong Kong Polytechnic University, Kowloon, Hong Kong SAR, China*

*Corresponding author.

Email: songcheng@polyu.edu.hk

Song Cheng

Phone: +852 2766 6668

Novelty and Significance Statement

This work presents a first-of-its-kind study that addresses two significant questions for RCM autoignition studies in the fundamental combustion community, which have been completely overlooked in the past: (1) Experiment-wise, can real-fluid behavior in RCMs affect interpretation and analysis of RCM experimental data? and (2) simulation-wise, can real-fluid behavior in RCMs affect RCM autoignition modeling and the validation of chemical kinetic models? Through the present study, we prove that real-fluid behavior in RCMs under common RCM test conditions is significant, and ignoring this can jeopardize the interpretation of RCM experimental data, introduce considerable error into RCM modeling results, and disqualify validation of chemical kinetic models. These issues can be addressed by the new approach proposed in this study, which fully captures the real-fluid behavior in RCMs, and shall be followed by future RCM autoignition studies (both experimental and modeling), particularly those at higher pressure conditions.

CRedit authorship contribution statement

Mingrui Wang: Writing – original draft, Conceptualization, Methodology, Formal analysis, Investigation. **S. Scott Goldsborough:** Methodology, Investigation, Writing – review & editing. **Song Cheng:** Writing – original draft, Conceptualization, Methodology, Formal analysis, Investigation, Writing – review & editing, Supervision, Funding acquisition.

Abstract

Rapid compression machines (RCMs) have been extensively used to quantify fuel autoignition chemistry and validate chemical kinetic models at high-pressure conditions. Historically, the analyses of experimental and modeling RCM autoignition data have been conducted based on the adiabatic core hypothesis with ideal gas assumption, where real-fluid behavior has been completely overlooked, though this might be significant at common RCM test conditions. This work presents a first-of-its-kind study that addresses two significant but completely overlooked questions for autoignition studies within RCMs in the fundamental combustion community: (i) Experiment-wise, can real-fluid behavior in RCMs affect interpretation and analysis of RCM experimental data? and (ii) simulation-wise, can real-fluid behavior in RCMs affect RCM autoignition modeling and the validation of chemical kinetic models? To this end, theories for real-fluid isentropic change are newly proposed and derived based on high-order Virial EoS, and are further incorporated into an effective-volume real-fluid autoignition modeling framework newly developed for RCMs. With detailed analyses, the strong real-fluid behavior in common RCM tests is confirmed, which can greatly influence the interpretation of RCM autoignition experiments, particularly the determination of end-of-compression temperature and evolution of the adiabatic core in the reaction chamber. Furthermore, real-fluid RCM modeling results reveal that considerable error can be introduced into simulating RCM autoignition experiments when following the community-wide accepted effective-volume approach with assuming ideal-gas behavior, which can be as high as 64% in the simulated ignition delay time at compressed pressure of 125 bar and lead to contradictory validation results of chemical kinetic models. Therefore, we recommend the community to adopt frameworks with real-fluid behavior fully accounted for (e.g., the one developed in this study) to analyze and simulate past and future RCM experiments, so as to avoid misinterpretation of RCM autoignition experiments and eliminate the potential errors that can be introduced into the simulation results with the existing RCM modeling frameworks.

Keywords: Rapid compression machine; Real-fluid behavior; Real-fluid isentropic relations; High-pressure autoignition; High-order Virial equation of state

1. Introduction

Rapid compression machines (RCMs) [1,2], where a single compression event is utilized to compress a prefilled mixture in the reaction chamber within 10-60 ms to a targeted high-pressure and high-temperature thermodynamic state, have a long history of application in combustion research. The uniqueness and advantage of RCM lie not only in the range of encompassed chemical timescales (e.g., 3 – 100 ms) and thermodynamic conditions (e.g., 500 – 1100 K in temperature) that compensate other types of fundamental combustion reactors (e.g., shock tube), but also in its convenient coupling with various diagnostic techniques, such as pressure and position transducers [3-5], off-line sampling [6, 7], online sampling [8], Schlieren imaging [9], particle image velocimetry [10], laser-induced imaging [11-14], etc., which make RCM an indispensable tool for both fundamental and applied combustion research at engine-relevant conditions.

Alongside many other applications (e.g., studying engine knock [15], characterizing heat release rates [16, 17], understanding non-ideal piston kinematics [5], unraveling turbulence-chemistry interactions [18], etc.), the most common use of RCMs is perhaps to study autoignition chemistry, thereby developing and validating chemical kinetic models that can be reliably applied to predictive combustion modeling. Obviously, the adequacy of the chemical kinetic models is premised on the fidelity in fuel chemistry represented therein, which is further premised on the interpretation of the physics involved during RCM autoignition tests (e.g., RCM facility effects and/or physical interactions [19]) and how sufficient these are represented in the modeling framework used to simulate RCM experiments. As such, there have been a number of approaches developed for modeling RCM experiments with various levels of fidelity.

Historically, RCMs was modelled as a homogeneous constant volume reactor with linearly described heat loss [20, 21]. It was quickly demonstrated that volumetrically averaged state conditions can not sufficiently represent the highly dynamic and reactive environment experienced in the reaction chamber [22], and that significant discrepancies can arise between the simulated results and experiments with this type of models. With such awareness, Keck and co-workers [23, 24] first hypothesized that autoignition chemistry

within the reaction chamber proceeds at faster rates within the hotter core portion of the mixture that is surrounded by the colder boundary layer. Based on this assumption, an adiabatic core was defined, which can be modeled as an adiabatic reactor with time-varying volume. Though there have been a few other extensions, e.g., CFD approaches [25], the variable-volume adiabatic core approach (now commonly known as the effective volume approach) has persisted as the basis for almost all 0-D RCM modeling over the past two decades.

Today, RCM autoignition studies have been following a consistent method to acquire two levels of information that are crucial for interpreting both experimental measurements and modeling results for RCMs. The first level of information is the end-of-compression temperature (T_{EOC}) that is used to mark the thermodynamic state for autoignition experiments and, particularly, for comparison of ignition reactivity among datasets reported by different groups (e.g., through Arrhenius diagrams). The second level of information is the rate of change in the adiabatic core volume during piston compression and the subsequent ignition delay periods, which is required by the effective volume approach to describe the heat loss characteristics from the adiabatic core to the surroundings during autoignition modeling. Both levels of information have been computed from the measured pressure data from a non-reactive test (obtained at identical initial conditions (e.g., temperature, pressure and composition) as the corresponding reactive test, while with O_2 in the test mixture replaced by N_2). However, such computations have all been conducted based on the ideal gas equation of state (EoS), in conjunction with the isentropic relations that have also been derived based on ideal gas assumption. In doing so, the real-fluid behavior in RCMs has been completely overlooked, despite the fact that RCMs have been increasingly used to study autoignition chemistry at high-pressure conditions (e.g., at above 100 bar for hydrocarbons [26] and gasoline fuels [27, 28]) where real-fluid effects might be significant. Unfortunately, efforts to characterize the real-fluid behavior in RCMs have not been available in the past and the real-fluid impact on the interpretation of RCM experiments and modeling results remain unknown.

In this article, we present results that, for the first time, confirm the strong real-fluid behavior in common RCM tests, and its significant influences on the interpretation of RCM autoignition experiments, particularly for the determination of end-of-compression temperature and evolution of the adiabatic core in the reaction chamber. Furthermore, we reveal the considerable error that can be introduced into simulating RCM autoignition experiments when following the community-wide accepted effective-volume approach with assuming ideal-gas behavior, which is found to be over 200% greater than those observed in other fundamental combustion reactors (e.g., shock tube) at similar pressure conditions. These discoveries are enabled through real-fluid isentropic expansion theories that are newly derived in this study and the supercritical modeling framework previously developed by our group [29-31] that is further modified herein to achieve variable volume simulations. This supercritical modeling framework couples *ab initio* intermolecular potentials, high-order mixture Virial EoS, real-fluid blending theories, real-fluid thermodynamics, and real-fluid combustion conservation laws, which has demonstrated impressive fidelity to reproduce real fluid properties during supercritical combustion modeling [29-31]. With the results obtained, we recommend the community to adopt frameworks with real-fluid behavior fully accounted for (e.g., the one developed in this study), to analyze and simulate past and future RCM experiments (particularly high-pressure experiments), so as to avoid misinterpretation of RCM autoignition experiments and the errors that can be introduced into the simulation results obtained from using the existing RCM modeling frameworks (e.g., the ideal effective volume approach).

2. Methodologies

2.1 Real-fluid isentropic relations

The isentropic change equations for ideal gas are given by:

$P\bar{v}^k = const$	(1)
$T\bar{v}^{(k-1)} = const$	(2)
$P^{(1-k)}T^k = const$	(3)

where \bar{v} is the molar volume and the k is the ratio of molar heat capacity at constant pressure to the molar heat capacity at constant volume: $k = \bar{c}_p/\bar{c}_v$. Previous RCM studies applied Eqs.1–3 and the ideal gas EoS over all of the experimental conditions including pre- and post-compression to calculate the volume and temperature histories based on known initial conditions. For instance, the end-of-compression temperature based on ideal gas adiabatic core hypothesis can be determined as:

$\int_{T_0}^{T_{EoC}} \frac{k}{k-1} \frac{dT}{T} = \ln \frac{P_{EoC}}{P_0}$	(4)
-----------------------------------------------------------------------------	-----

where the subscripts ‘0’ and ‘EoC’ indicate initial and compressed conditions.

For real fluids, it can be reasonably assumed that the isentropic change equations follow the same form as those for ideal gas, while with different isentropic exponents. Therefore, the real-fluid isentropic change equations can be written as:

$P\bar{v}^{k_{p\bar{v}}} = const$	(5)
$T\bar{v}^{(k_{T\bar{v}}-1)} = const$	(6)
$P^{(1-k_{pT})}T^{k_{pT}} = const$	(7)

where $k_{p\bar{v}}$, $k_{T\bar{v}}$, and k_{pT} are the real-fluid isentropic exponents governing $P - \bar{v}$, $T - \bar{v}$, and $P - T$ relationship, respectively.

To derive the expressions for the real-fluid isentropic exponents $k_{p\bar{v}}$, $k_{T\bar{v}}$, and k_{pT} , taking logarithms and differentiating Eqs.5–7 yields:

$\frac{dP}{P} + k_{p\bar{v}} \frac{d\bar{v}}{\bar{v}} = 0$	(8)
$\frac{dT}{T} + (k_{T\bar{v}} - 1) \frac{d\bar{v}}{\bar{v}} = 0$	(9)
$(1 - k_{pT}) \frac{dP}{P} + k_{pT} \frac{dT}{T} = 0$	(10)

By rearranging Eqs.8–10, the differential changes of P , T , and \bar{v} for a real-fluid isentropic system are expressed as:

$\left(\frac{\partial P}{\partial \bar{v}}\right)_s = -k_{p\bar{v}} \frac{P}{\bar{v}}$	(11)
$\left(\frac{\partial T}{\partial \bar{v}}\right)_s = -(k_{T\bar{v}} - 1) \frac{T}{\bar{v}}$	(12)

$\left(\frac{\partial P}{\partial T}\right)_{\bar{s}} = \frac{k_{pT} P}{k_{pT} - 1 T}$	(13)
----------------------------------------------------------------------------------------	------

During non-reactive experiments, the mole fraction of each component remains unchanged, and the mixture entropy can be expressed with respect to two independent variables such as T and P , or \bar{v} and P . According to the fundamental thermodynamic relation and Maxwell's relations, the entropy changes in an isentropic system are stated as:

$d\bar{s} = \left(\frac{\partial \bar{s}}{\partial T}\right)_P dT + \left(\frac{\partial \bar{s}}{\partial P}\right)_T dP = \bar{c}_p \frac{dT}{T} - \left(\frac{\partial \bar{v}}{\partial T}\right)_P dP = 0$	(14)
-----------------------------------------------------------------------------------------------------------------------------------------------------------------------------------------------------------------	------

$d\bar{s} = \left(\frac{\partial \bar{s}}{\partial P}\right)_{\bar{v}} dP + \left(\frac{\partial \bar{s}}{\partial \bar{v}}\right)_P d\bar{v} = \bar{c}_v \frac{dT}{T} + \left(\frac{\partial P}{\partial T}\right)_{\bar{v}} d\bar{v} = 0$	(15)
---------------------------------------------------------------------------------------------------------------------------------------------------------------------------------------------------------------------------------------------	------

Rearranging Eq.14 and Eq.15 yields the formulas of differential changes $\left(\frac{\partial T}{\partial \bar{v}}\right)_{\bar{s}}$ and $\left(\frac{\partial P}{\partial T}\right)_{\bar{s}}$:

$\left(\frac{\partial T}{\partial \bar{v}}\right)_{\bar{s}} = -\frac{T}{\bar{c}_v} \left(\frac{\partial P}{\partial T}\right)_{\bar{v}}$	(16)
------------------------------------------------------------------------------------------------------------------------------------------	------

$\left(\frac{\partial P}{\partial T}\right)_{\bar{s}} = \frac{\bar{c}_p}{T} \left(\frac{\partial T}{\partial \bar{v}}\right)_P$	(17)
---------------------------------------------------------------------------------------------------------------------------------	------

Combining Eq.16 and Eq.17, the differential change $\left(\frac{\partial P}{\partial \bar{v}}\right)_{\bar{s}}$ can be obtained:

$\left(\frac{\partial P}{\partial \bar{v}}\right)_{\bar{s}} = \frac{(\partial P/\partial T)_{\bar{s}}}{(\partial \bar{v}/\partial T)_{\bar{s}}} = -\frac{\bar{c}_p}{\bar{c}_v} \left(\frac{\partial T}{\partial \bar{v}}\right)_P \left(\frac{\partial P}{\partial T}\right)_{\bar{v}}$	(18)
-----------------------------------------------------------------------------------------------------------------------------------------------------------------------------------------------------------------------------------------------------------------------------------------	------

The triple product rule gives the relation between P , T , and \bar{v} as $\left(\frac{\partial \bar{v}}{\partial P}\right)_T \left(\frac{\partial T}{\partial \bar{v}}\right)_P \left(\frac{\partial P}{\partial T}\right)_{\bar{v}} = -1$, based on which Eq.18 can be written as:

$\left(\frac{\partial P}{\partial \bar{v}}\right)_{\bar{s}} = \frac{\bar{c}_p}{\bar{c}_v} \left(\frac{\partial P}{\partial \bar{v}}\right)_T$	(19)
-----------------------------------------------------------------------------------------------------------------------------------------------	------

As the right-hand sides (RHS) of Eq.11 and Eq.19, of Eq.12 and Eq.16, and of Eq.13 and Eq.17 are equal, the generalized isentropic exponents for real fluids are expressed as:

$k_{p\bar{v}} = -\frac{\bar{v} \bar{c}_p}{P \bar{c}_v} \left(\frac{\partial P}{\partial \bar{v}}\right)_T$	(20)
------------------------------------------------------------------------------------------------------------	------

$k_{T\bar{v}} = 1 + \frac{\bar{v}}{\bar{c}_v} \left(\frac{\partial P}{\partial T}\right)_{\bar{v}}$	(21)
-----------------------------------------------------------------------------------------------------	------

$k_{pT} = \frac{1}{1 - \frac{P}{\bar{c}_p} \left(\frac{\partial \bar{v}}{\partial T}\right)_P}$	(22)
-------------------------------------------------------------------------------------------------	------

The RHS of Eqs.20–21 should then be determined based on a real-fluid EoS, instead of the ideal gas EoS. Following the previous studies from our group [29-31], high-order Virial EoS is adopted due to its superiority to quadratic and cubic EoS, which can be expressed as:

$\frac{P\bar{v}}{RT} = 1 + \frac{B_2}{\bar{v}} + \dots + \frac{B_N}{\bar{v}^{(N-1)}}$	(23)
---------------------------------------------------------------------------------------	------

where B_2, \dots, B_N are the second, ..., and N^{th} -order Virial coefficients which represent intermolecular interactions between two molecules, ..., and N molecules, respectively, in the real fluid.

Taking partial derivatives of Eq.23 with respect to \bar{v} and T , respectively, yielding:

$\left(\frac{\partial P}{\partial \bar{v}}\right)_T = -\frac{RT}{\bar{v}^2} \left(1 + \frac{2B_2}{\bar{v}} \dots + \frac{NB_N}{\bar{v}^{(N-1)}}\right)$	(24)
---------------------------------------------------------------------------------------------------------------------------------------------------------	------

$\left(\frac{\partial P}{\partial T}\right)_{\bar{v}} = R \left(\frac{1}{\bar{v}} + \frac{B_2 + T \frac{\partial B_2}{\partial T}}{\bar{v}^2} + \dots + \frac{B_N + T \frac{\partial B_N}{\partial T}}{\bar{v}^N}\right)$	(25)
---------------------------------------------------------------------------------------------------------------------------------------------------------------------------------------------------------------------------	------

Substituting Eq.24 and Eq.25 into Eq.20 and Eq.21, respectively, the real-fluid isentropic exponents $k_{p\bar{v}}$ and $k_{T\bar{v}}$ based on the N^{th} -order Virial EoS are ultimately given by:

$k_{p\bar{v}} = RT \frac{\bar{v} \bar{c}_p}{p \bar{c}_v} \frac{1}{\bar{v}^2} \left(1 + \frac{2B_2}{\bar{v}} \dots + \frac{NB_N}{\bar{v}^{(N-1)}}\right)$	(26)
----------------------------------------------------------------------------------------------------------------------------------------------------------	------

$k_{T\bar{v}} = 1 + R \frac{\bar{v}}{\bar{c}_v} \left(\frac{1}{\bar{v}} + \frac{B_2 + T \frac{\partial B_2}{\partial T}}{\bar{v}^2} + \dots + \frac{B_N + T \frac{\partial B_N}{\partial T}}{\bar{v}^N}\right)$	(27)
-----------------------------------------------------------------------------------------------------------------------------------------------------------------------------------------------------------------	------

The third real-fluid isentropic exponent, k_{pT} , is not independent, as indicated by Eq.20–22, which can be calculated using:

$\frac{k_{p\bar{v}}}{k_{T\bar{v}} - 1} = \frac{k_{pT}}{k_{pT} - 1}$	(28)
---------------------------------------------------------------------	------

Combining Eq.26 with Eq.20 and integrating Eq.20 from the initial condition at $t = 0$, the real-fluid molar volume of the adiabatic core can be determined from measured non-reactive pressure traces. Similarly, combining Eq.27 with Eq.21, and integrating Eq.21 from the initial condition at $t = 0$ yields the real-fluid adiabatic core temperature, from which real-fluid T_{EoC} can be determined.

2.2 Real-fluid autoignition modeling in RCMs

In this study, the simulations of RCM autoignition with real-fluid behavior are conducted using the supercritical autoignition modeling module in the UHPC_RF_Master 1.0 package, while with further modifications as discussed below. Details of the supercritical autoignition modeling framework have already been comprehensively summarized in [29, 32], including the computation of high-order pure Virial coefficients for both radicals and stable species, mixture high-order Virial coefficients, and real-fluid thermodynamics, hence will not be discussed herein. Nevertheless, it is important to note that the supercritical autoignition modeling framework was used for autoignition modeling in shock tubes in the previous studies [29, 32], which did not consider a compression process or any heat loss. Modeling RCMs presents itself with additional complexity than shock tubes, where compression exothermicity, compression and post-compression heat loss, and machine operation nuances (e.g., piston creep and rebound) need to be sufficiently captured during modeling. To capture these, the adiabatic core hypothesis is still adopted using the effective volume approach, where the core gas thermodynamic states are determined based on real-fluid thermodynamic partition functions and high-order mixture Virial EoS. In fact, when developing the supercritical autoignition modeling framework in [29, 32], the open control volume was already conceptualized as a homogeneous non-adiabatic reactor with varying volume. The modeling of supercritical autoignition in shock tubes was then conducted by setting the volume at the fixed value and the rate of volume change ($\frac{dV}{dt}$) and heat loss ($\frac{dQ}{dt}$) as zero, thereby converting the homogeneous non-adiabatic reactor with varying volume into a homogeneous adiabatic constant-volume reactor. In this study, the heat loss term (i.e., $\frac{dQ}{dt}$ in Eq.25 in [29]) is still set at zero, while the control volume is allowed to change its volume to represent a volume-varying adiabatic core. This is achieved by re-activating the V and $\frac{dV}{dt}$ terms in the real-fluid combustion governing equations (e.g., the last term on the RHS of Eq.25 in [29]). The V and $\frac{dV}{dt}$ are computed from Eq.26 and Eq.20 with integration starting from $t = 0$ using the pressure data from the non-reactive experiments.

On the other hand, the supercritical autoignition modeling framework requires the Virial coefficients to be determined for all chemical species defined in a chemistry set (i.e., a chemical kinetic model). In this study, the NUIGMech1.1 [33] is used, for which the Virial coefficients for all species have already been computed in our previous study [32].

Simulations of ideal gas autoignition in RCM are conducted following the conventional effective volume approach with volume-time histories derived based on ideal gas assumption. The simulations are performed using the LLNL-developed fast solver ZeroRK [34], with ideal volume profiles included to account for compression and heat loss [28].

The conditions and mixture covered in this study are summarized in Table 1, which are the experimental conditions reported by Ramalingam et al. [35]. To the authors' knowledge, this RCM dataset has the highest compressed pressure conditions (i.e., up to 160 bar) among all existing RCM studies that reported non-reactive experimental pressure data. As real-fluid behavior typically gets stronger at high-pressure conditions, this dataset is ideal for investigating the real-fluid behavior and its impact in RCMs.

Table 1 Experimental conditions for real-fluid RCM autoignition modeling in this study. Experiments are from [35].

Case No.	Composition*	X _{CH4}	X _{C2H6}	Φ	D (%)	T ₀ (K)	P ₀ (bar)	T _{EoC} (K) [^]	P _{EoC} (bar)
1	CH ₄ /AR/N ₂	4.19	0	0.417	75.7	294.6-296.3	3.16-3.34	888-936	125
2	CH ₄ /AR/N ₂	4.74	0	0.526	77.3	294.7-296.4	2.64-2.76	894-938	105
3	CH ₄ /AR/N ₂	4.74	0	0.526	77.3	294.6-297.1	3.15-3.28	895-937	125
4	CH ₄ /AR/N ₂	4.74	0	0.526	77.3	298.2-299.0	2.76-2.88	887-922	150
5	CH ₄ /AR/N ₂	5.24	0	0.526	75.0	294.6-297.0	3.19-3.32	886-933	125
6	CH ₄ /AR/N ₂	6.63	0	1.000	80.1	296.1-296.9	2.97-3.06	893-926	160
7	CH ₄ /C ₂ H ₆ /AR/N ₂	4.17	0.62	0.526	75.0	296.6-296.8	2.38-2.48	890-933	125

* O₂ is replaced with N₂ in non-reactive tests and used for computing volume-time histories;

[^] T_{EoC} computed based on ideal gas assumption

3. Results and discussion

3.1. Real-fluid isentropic change

The first question we explore is whether the real-fluid isentropic change proceeds in a different manner from the ideal one. To answer this question, the three real-fluid isentropic exponents (i.e., $k_{p\bar{v}}$, $k_{T\bar{v}}$, and k_{pT}) and the ideal isentropic exponent (i.e., k) for the mixture and condition of Case 5 are computed, with the results summarized in Fig. 1. We

find that the real-fluid isentropic exponents computed from high-order mixture Virial EoS and real-fluid isentropic change theories differ greatly from each other, as well as from the ideal isentropic exponent. Among the three real-fluid isentropic exponents, only k_{pT} follows a similar trend as the ideal exponent, while the others are obviously greater over the entire compression and the post-compression periods. These differences are expected to shift the thermodynamic evolution of the adiabatic core away from that determined based on the ideal gas assumption.

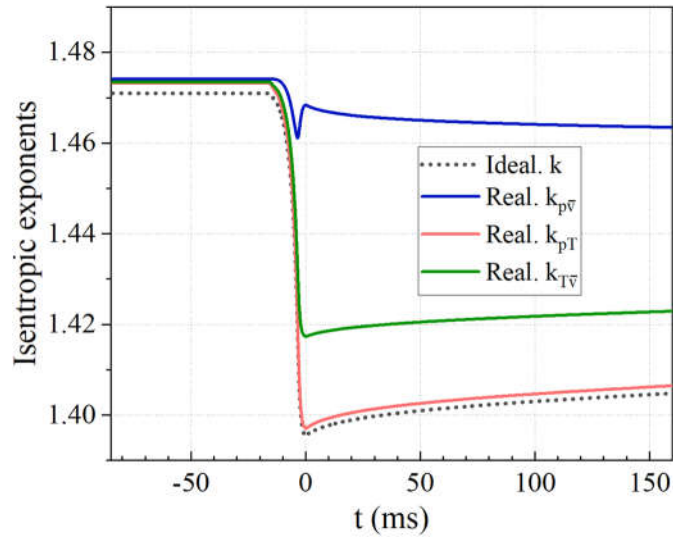


Figure 1. Computed ideal and real-fluid isentropic exponents during the non-reactive simulation for Case 5 at $T_0=295.8$ K and $P_0=3.32$ bar.

3.2. Real-fluid effects on evolution of adiabatic core and interpretation of RCM experiments

Given the results in Fig. 1, the impact of real-fluid behavior on the evolution of adiabatic core is further investigated. This is achieved by computing the thermodynamic states of the adiabatic core during the non-reactive experiments, following the approach outlined in Section 2. Figure 2 illustrates the changes in adiabatic core volume and temperature (relative to ideal gas adiabatic core) when real-fluid effects are considered during the non-reactive modeling for Case 5. As can be seen in Fig. 2, as the compression starts, the real-fluid effects rapidly increase the volume and temperature of the adiabatic core, reaching the largest rise in these properties at the end of compression (about 4.5% in volume and 0.32% in temperature). Following this point, real-fluid effects still impose positive impacts, with the

impact gradually decreasing over time. It is important to recognize that these changes are not a form of uncertainty, but rather a source of error that will be introduced into data analysis when ignoring real-fluid effects. Given that the typical level of uncertainty in computed T_{EoC} is within 1% [36], an addition error of 0.32% could increase the uncertainty in computed T_{EoC} by more than 30%, a significant value that should certainly be eliminated.

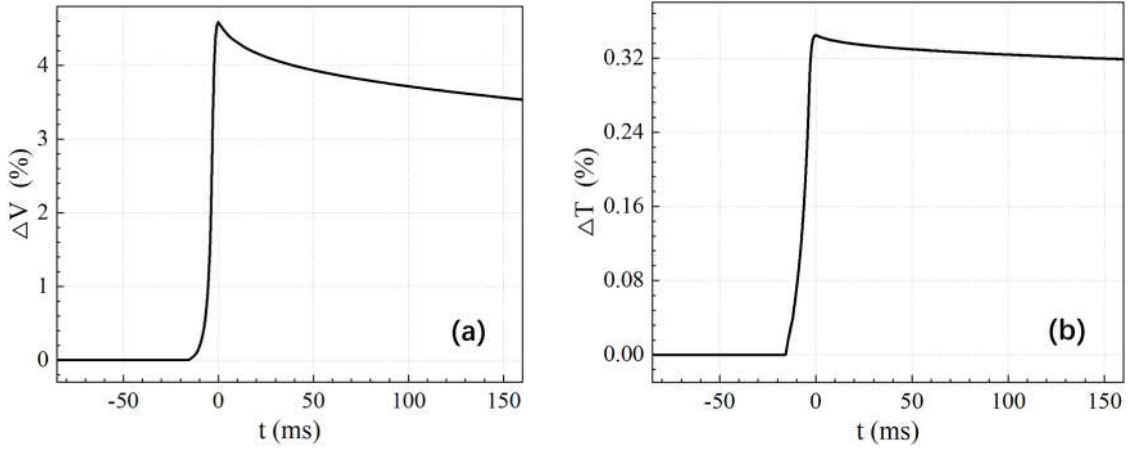


Figure 2. Real-fluid effects on the evolution of adiabatic core during the non-reactive simulation for Case 5 at $T_0=295.8$ K and $P_0=3.32$ bar: (a) Difference in adiabatic core volume between the ideal and real-fluid calculations, computed as $\Delta V = (V_{Real} - V_{Ideal})/V_{Ideal}$; (b) difference in adiabatic core temperature between the ideal and real-fluid calculations, computed as, $\Delta T = (T_{Real} - T_{Ideal})/T_{Ideal}$.

Figure 3 further shows the real-fluid effects on the molar enthalpy (\bar{h}) and molar heat capacity (\bar{c}_p) of the adiabatic core. The evolution of real-fluid adiabatic core with respect to its \bar{h} and \bar{c}_p also differs from the ideal gas adiabatic core, following similar trends as those seen in Fig. 2. At the end of compression, real-fluid effects can increase the \bar{h} of the adiabatic core by approximately 150 J/mol, and \bar{c}_p by more than 0.4 J/mol/K, revealing the strong impact of real-fluid behavior on the thermodynamic evolution of the adiabatic core.

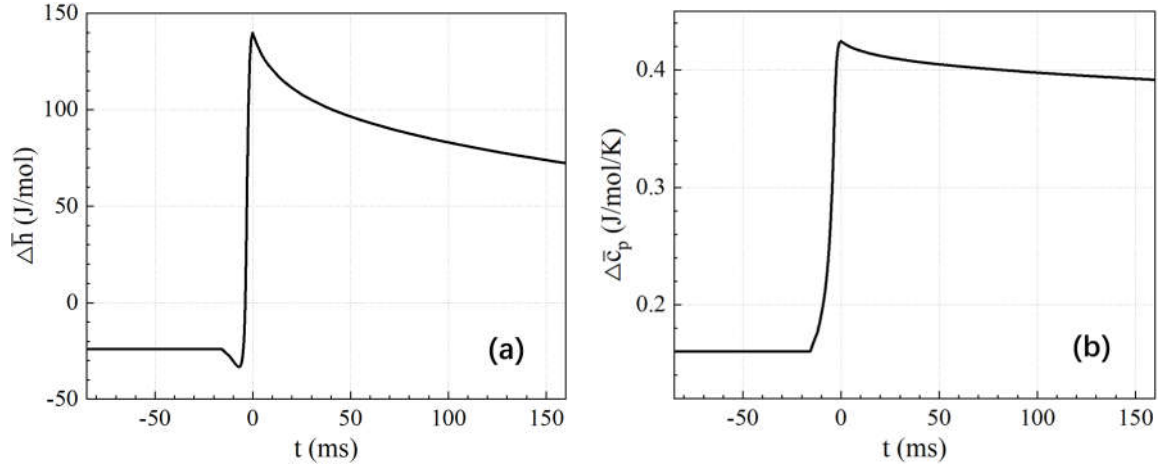


Figure 3. Real-fluid effects on the evolution of adiabatic core during the non-reactive simulation for Case 5 at $T_0=295.8$ K and $P_0=3.32$ bar: (a) Difference in adiabatic core molar enthalpy between the ideal and real-fluid calculations, computed as $\Delta\bar{h} = (\bar{h}_{Real} - \bar{h}_{Ideal})/\bar{h}_{Ideal}$; (b) Difference in adiabatic core molar heat capacity at constant pressure between the ideal and real-fluid calculations, $\Delta\bar{c}_p = (\bar{c}_{p,Real} - \bar{c}_{p,Ideal})/\bar{c}_{p,Ideal}$.

With the strong impact confirmed in Figs. 2 and 3, the real-fluid effects on the determination of T_{EoC} are further characterized for only Case 5 in Fig. 2b to all 7 cases covered in this study. The results are summarized in Fig. 4, where the error that can be introduced into the computed T_{EoC} is plotted against the T_{EoC} determined based on ideal gas assumption. Immediately seen in Fig. 4 is the prominent change in T_{EoC} after considering real-fluid behavior, where the T_{EoC} will be consistently underestimated if real-fluid effects are not considered. The level of error in T_{EoC} increases linearly with decreasing temperature, while increasing non-linearly with pressure at a relatively higher rate compared to that seen for temperature. The highest error in T_{EoC} for the conditions investigated in this study reaches above 3 K at $T_{EoC,Ideal} = \sim 890$ K. This error rivals the typical levels of uncertainty in computed T_{EoC} in RCMs, which was estimated at 2 – 5 K at $T_{EoC,Ideal}$ of 810 – 1062 K, as reported in [36].

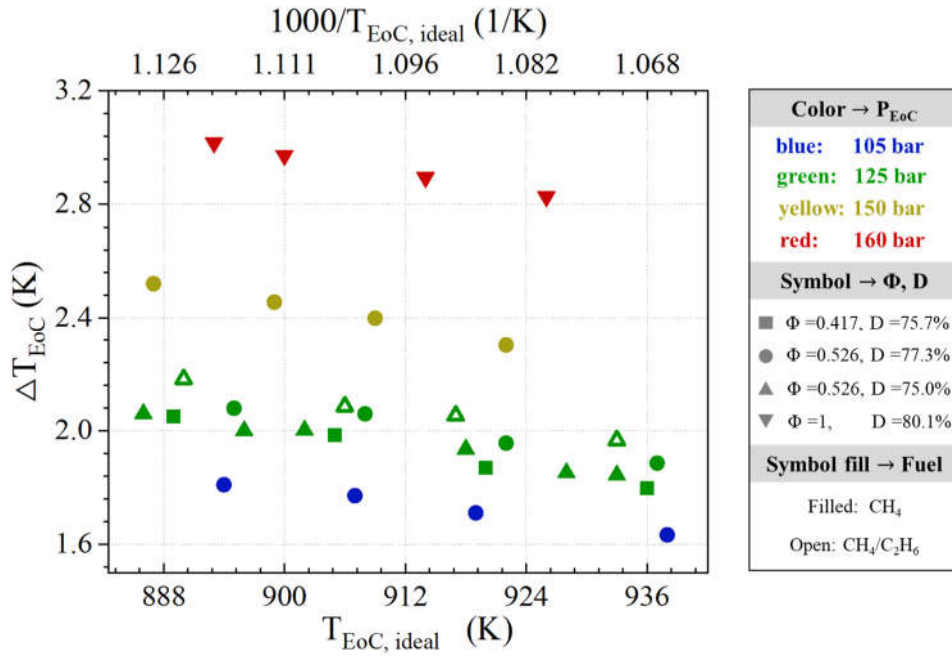


Figure 4. Real-fluid effects on the determination of T_{EoC} for various fuel mixtures at T_{EoC} =886-939 K, P_{EoC} =105-160 bar, Φ =0.417-1.000, and D =75.7%-80.1% (covering Cases 1-7), quantified by $\Delta T_{EoC} = T_{EoC,Real} - T_{EoC,Ideal}$, where $T_{EoC,Real}$ and $T_{EoC,Ideal}$ are calculated using the real-fluid modeling framework in this study and based on ideal gas assumption, respectively.

The errors introduced into T_{EoC} will certainly lead to misinterpretation of RCM autoignition experiments. This is directly illustrated in Fig. 5. As can be seen in Fig. 5, with the corrected T_{EoC} (namely $T_{EoC,Real}$), the Arrhenius plots for ignition delay times are all shifted towards higher temperatures, and the shifted Arrhenius plots exhibit stronger temperature dependence due to the greater error in T_{EoC} at lower temperatures. These changes in Arrhenius plots can jeopardize RCM analysis in many ways, such as (i) the characterization of NTC (negative temperature coefficient) region that is often defined as a range of T_{EoC} and (ii) comparisons of different RCM datasets from various groups that is often conducted with respect to T_{EoC} .

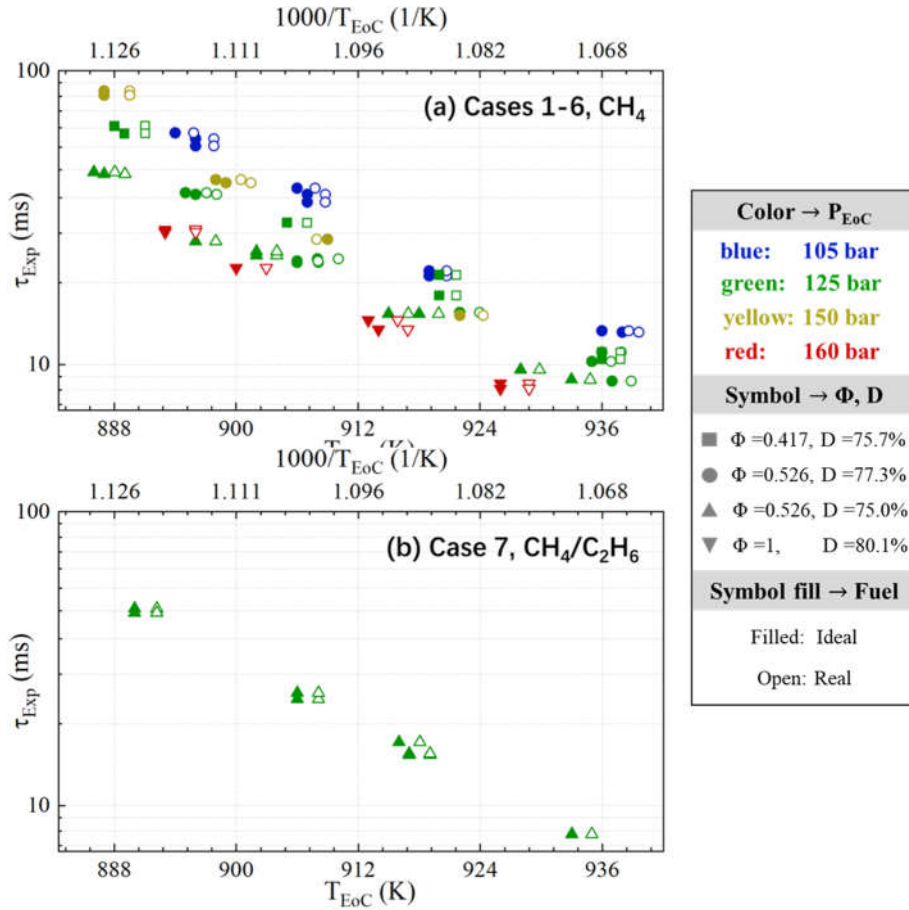


Figure 5. Shift in the Arrhenius diagrams of measured ignition delay times vs. T_{EoC} after considering real-fluid effects: (a) Fuel CH_4 (Cases 1-6); (b) Fuel CH_4/C_2H_6 (Case 7).

3.3. Real-fluid effects on RCM autoignition simulation

Further to the results in Section 2 that confirm the impact of real-fluid behavior on RCM experimental data analysis and interpretation, in this section, we explore the effects that real-fluid behavior can exert on RCM autoignition simulation. We expect these effects in RCM to be more intense than those previously observed in shock tubes [29, 32], due to the coupling between compression and chemical kinetics, and the longer timescales in RCMs for real-fluid behavior to take effect.

Figure 6 shows the simulated reactive temperature- and pressure-time histories for Case 5 with (obtained using the modeling framework developed by us, as detailed in Section 2) and without (obtained using Zero-RK) real-fluid behavior incorporated. With considering real-fluid behavior from the start of compression, it is obvious from Fig. 6 that the temperature and pressure rise at a faster rate than the ideal case after the end of compression, which is followed by a greatly advanced ignition.

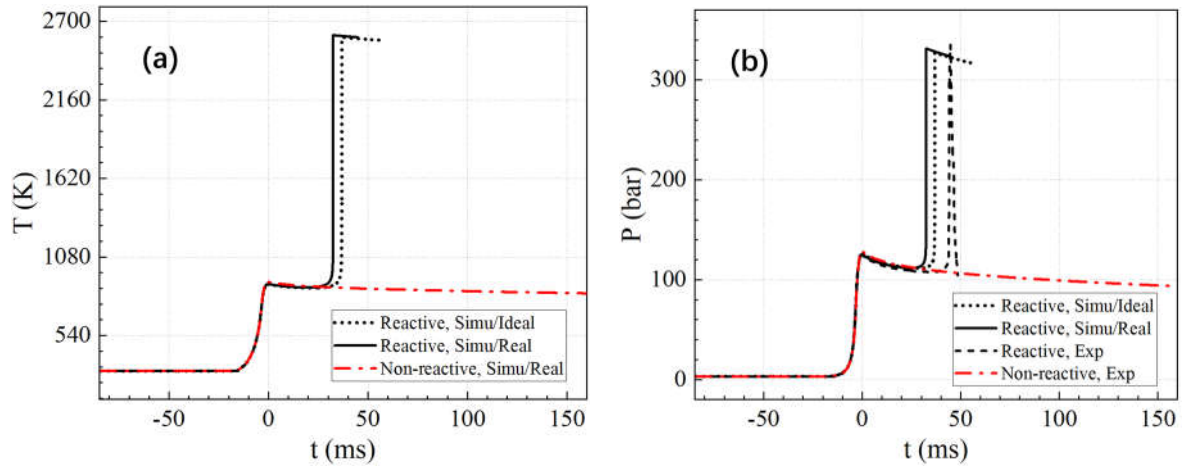


Figure 6. Simulated (a) temperature-time and (b) pressure-time histories for Case 5 at $T_0=295.8$ K and $P_0=3.32$ bar (Case 5) with (denoted as “Real”) and without (denoted as “Ideal”) considering real-fluid effects, along with the experiments from [35].

Ideal and real-fluid simulations are therefore conducted for all cases (c.f. Table 1) at all conditions covered, with the simulated ignition delay times displayed in Fig. 7 in an Arrhenius manner, along with the experimental data reported in [35]. The real-fluid simulation results start from a higher temperature than the ideal simulations, as the real-fluid ignition delay times are plotted against $T_{EoC,Real}$, while the ideal ones are plotted against $T_{EoC,Ideal}$. The experimental data in Fig. 7 are also corrected using $T_{EoC,Real}$ (as discussed in Section 3.2). Obviously seen in Fig. 7 is the strong impact of real-fluid behavior on RCM autoignition modeling results, where the real-fluid behavior consistently promotes ignition reactivity, leading to smaller predicted ignition delay times.

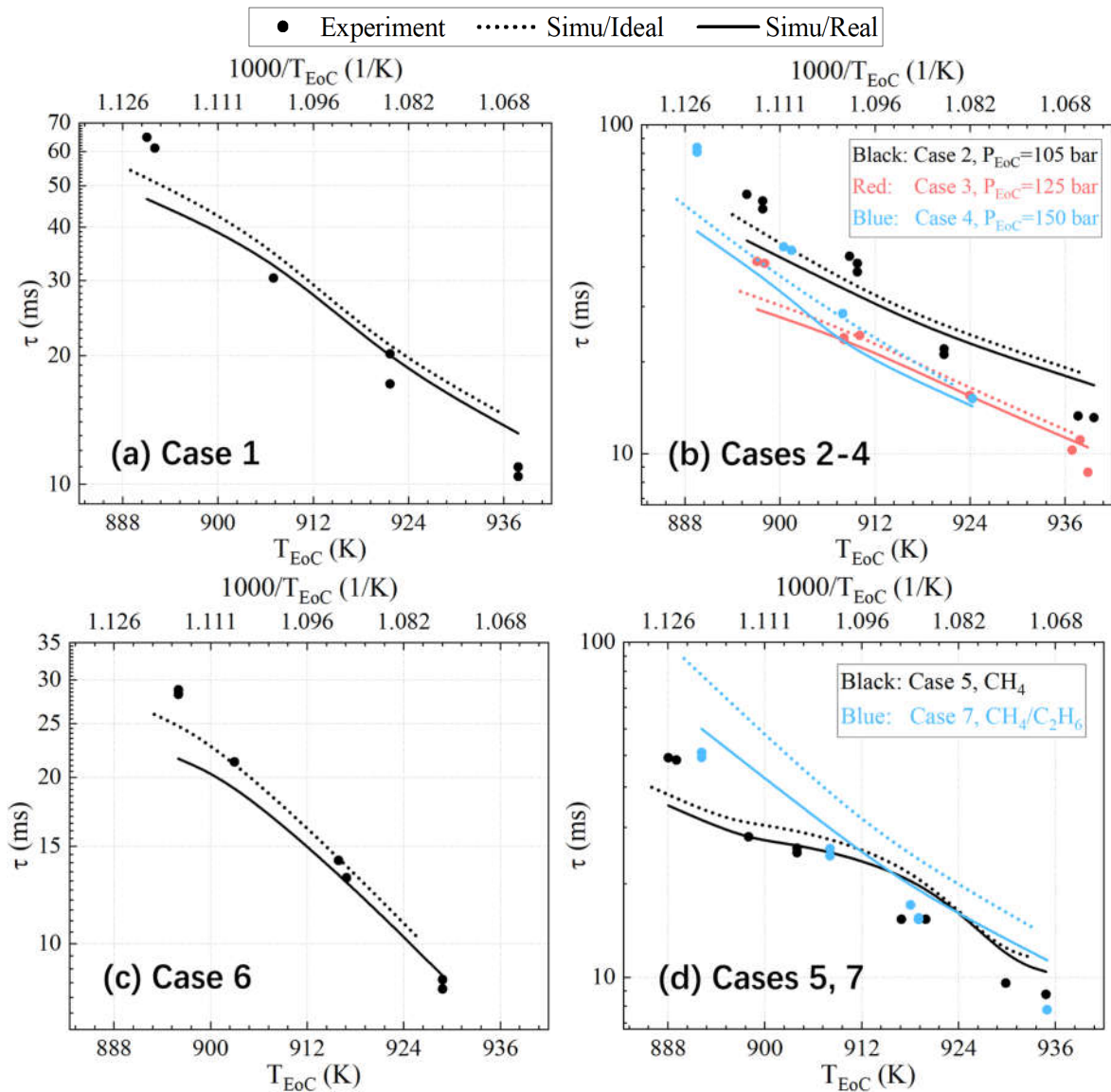


Figure 7. Simulated ignition delay time for Cases 1-7 with and without considering real-fluid effects, along with the experiments from [35]. The experiments and ideal simulation results are plotted against $T_{EoC,Ideal}$, while real-fluid simulation results and experiments are plotted against $T_{EoC,Real}$.

The change in simulated ignition delay times between the real-fluid and ideal RCM autoignition simulations is better quantified in Fig. 8. The error presented in simulated RCM ignition delay times reaches as high as 64% (i.e., Case 7 at 125 bar and ~ 890 K), which is substantially greater than those observed in shock tubes at similar pressure conditions (e.g., approximately 10% at similar pressure, as reported in [29, 32]). With this level of error introduced into the simulated ignition delay times, the comparisons between simulated and experimental autoignition results can be meaningless, and that the chemical kinetic models validated under such errors might not bear any practical value. An example can be seen in Fig. 7c. At $T_{EoC} = 916$ K, the ideal simulation results indicate that the chemical kinetic model

underestimates the ignition reactivity as compared to the experimental measurements. One would often increase the model reactivity to match the model better with experiments. However, with real-fluid corrections, the modeling results indicate that the model reactivity has been overestimated and should be tuned down rather than being increased (as would have been done with the conventional modeling approach). It is also interesting to see from Fig. 8 that with chemical kinetics coupled, the real-fluid effects are no longer monotonically dependent on pressure, while monotonical dependence of real-fluid effects on pressure has been observed in Fig. 4. This is the most obvious at compressed temperatures below 906 K, as well as for Case 7 where the strongest real-fluid effects are observed, though at a compressed pressure of 125 bar. These trends are consistent with the observations from our previous study [29], which both confirm that real-fluid effects are complicated and combined effects from various and, sometimes, competing contributors featured by different types of molecules including fuel species, radicals and diluents.

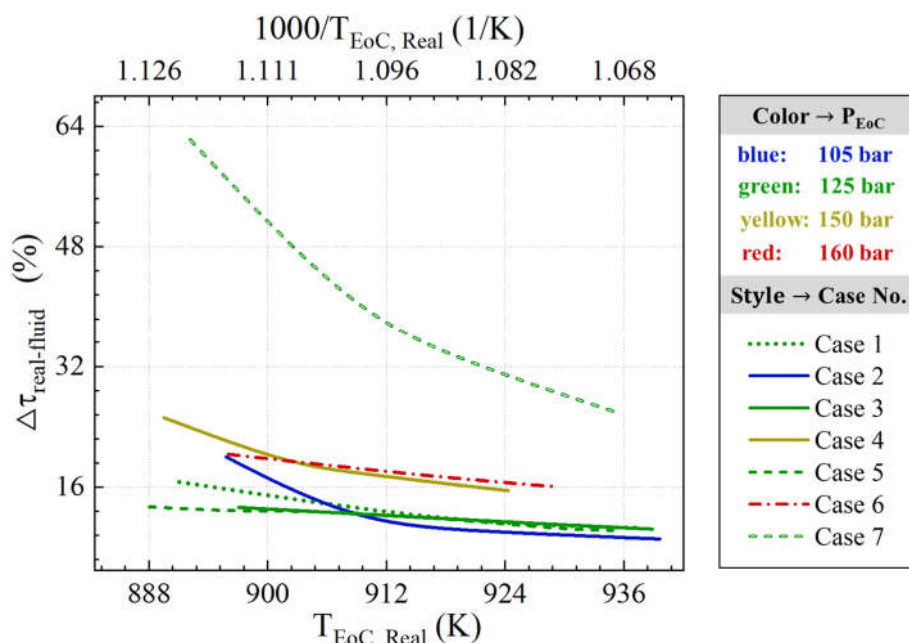


Figure 8. Real-fluid effects on autoignition simulation results for various fuel mixtures at $T_{EoC}=886-939$ K, $P_{EoC}=105-160$ bar, $\Phi=0.417-1$, and $D=75.7\%-80.1\%$ (covering Cases 1-7), quantified as $\Delta\tau_{real-fluid} = (\tau_{Ideal} - \tau_{Real})/\tau_{Real}$.

3.4. Decoupling of compression and post-compression real-fluid effects

The final question we explore is whether the contribution of the real-fluid behavior during compression can be decoupled from that after compression and during the delay period where strong chemical kinetics present, and if so, how significant is each contributor to the overall real-fluid effects. To answer these questions, the non-reactive pressure data is truncated at the end of compression, with the compression part used for real-fluid computation of volume profiles and the delay part used for idea computation of volume profiles (the last data point from the real-fluid compression part is used as the initial condition for the ideal computation in the delay part). This hybrid volume profile is then used for autoignition modeling. The simulated pressure-time histories from the ideal, hybrid, and real-fluid RCM autoignition simulations for Case 4 are shown in Fig. 9, where the difference between the hybrid and ideal results reflects the contribution of the compression real-fluid behavior to the total real-fluid effects, while the difference between the hybrid and real-fluid results indicates the contribution from the real-fluid behavior during the delay period. It can be seen from Fig. 9 that the compression real-fluid behavior is significant, which facilitates ignition reactivity by about half of the total real-fluid effects on autoignition reactivity for Case 4.

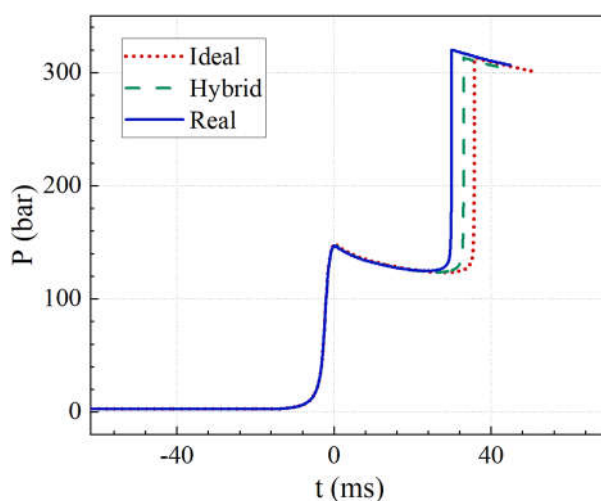


Figure 9. Simulated pressure-time histories for Case 4 at $T_0=298.9$ K and $P_0=2.85$ bar. Ideal – ideal simulation results; Hybrid – simulation results with only compression real-fluid behavior considered; Real – real-fluid simulation results.

The results in Fig. 9 are limited to Case 4, which might shift under other mixtures and thermodynamic conditions. To ascertain this, hybrid simulations are further conducted for all

thermodynamic conditions covered in Cases 2 – 4. The simulated ignition delay times from the ideal, hybrid, and real-fluid modeling are presented in Fig. 10 as functions of compressed temperatures (either $T_{EoC,Real}$ or $T_{EoC,Ideal}$). Over all conditions covered in Fig. 10, it is clear that the real-fluid behavior during compression process presents itself as a significant contributor to the total real-fluid effects on autoignition modeling, though relatively less significant compared to the real-fluid behavior during the delay period.

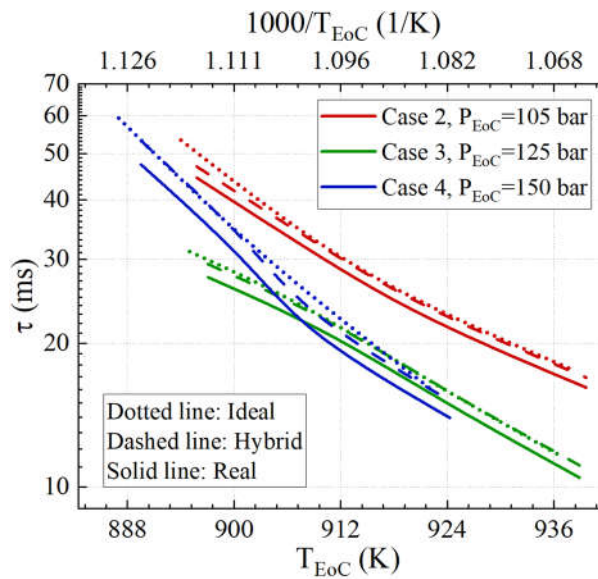


Figure 10. Simulated ignition delay times for Cases 2-4 at $T_{EoC}=887-939$ K, $P_{EoC}=105-150$ bar, $\Phi=0.526$, and $D=77.3\%$. Ideal – ideal simulation results plotted against $T_{EoC,Ideal}$; Hybrid – simulation results with only compression real-fluid behavior considered plotted against $T_{EoC,Real}$; Real – real-fluid simulation results plotted against $T_{EoC,Real}$.

Finally, Fig. 11 quantifies the relative contribution of compression real-fluid behavior to the total real-fluid effects on simulated ignition delay times, computed as $(\tau_{hybrid} - \tau_{Ideal})/(\tau_{Real} - \tau_{Ideal})$. The results in Fig. 11 confirm that the real-fluid effects in RCMs is dominated by the real-fluid behavior during the delay periods where stronger chemical kinetics present, rather than the compression period. Nevertheless, the real-fluid behavior during compression is still significant, which can contribute to over 50% of the overall real-fluid effects (e.g., Case 2 at T_{EoC} of 894 K, as seen in Fig. 11).

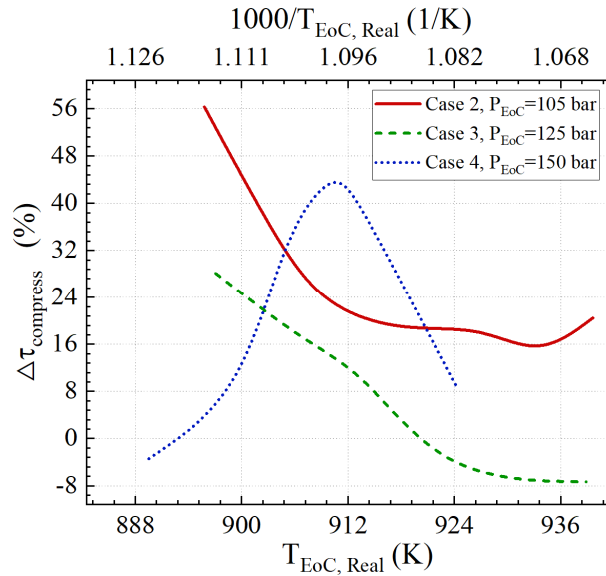


Figure 11. Relative contribution of the real-fluid behavior during compression to total real-fluid effects on simulated ignition delay times, quantified as $\Delta\tau_{compress} = (\tau_{hybrid} - \tau_{ideal})/(\tau_{Real} - \tau_{ideal})$. Simulations are conducted with $\text{CH}_4/\text{O}_2/\text{AR}/\text{N}_2$ mixtures at $T_{EoC}=887\text{-}939$ K, $P_{EoC}=105\text{-}150$ bar, $\Phi=0.526$, and $D=77.3\%$ (Cases 2-4).

Conclusions

This study presents the first-of-its-kind results to address two significant but completely overlooked questions for RCM autoignition studies in the fundamental combustion community: (1) Experiment-wise, can real-fluid behavior in RCMs affect interpretation and analysis of RCM experimental data? and (2) simulation-wise, can real-fluid behavior in RCMs affect RCM autoignition simulations and thus the validation of chemical kinetic models? To this end, theories for real-fluid isentropic change are newly proposed and derived based on high-order Virial EoS, which is further incorporated into an effective-volume supercritical autoignition modeling framework that is newly developed for modeling real-fluid autoignition in RCMs. The key findings of this study are:

- Real-fluid isentropic change proceeds in a greatly different manner from the ideal isentropic change.
- Real-fluid behavior reshapes the thermodynamic evolution of the adiabatic core in RCMs that could affect both experimental and modeling analysis in RCM studies.
- Ignoring real-fluid behavior leads to significant errors in computed end-of-compression temperature in RCMs that are comparable to typical levels of

computation uncertainties for T_{EOC} . These errors can mislead the interpretation of RCM experimental data.

- Real-fluid behavior considerably facilitates the simulated autoignition reactivity in RCMs, exhibiting strong dependences on mixture compositions and temperature and pressure conditions, with the promoting effect in RCMs being over 200% stronger than that observed in shock tubes at similar pressure conditions.
- Ignoring real-fluid behavior results in errors in simulated ignition delay times in RCMs that exceed typical levels of measurement uncertainty for ignition delay times, which can lead to contradictory validation results for chemical kinetic models.
- Real-fluid behavior during the ignition delay period, rather than that during compression, dominates the real-fluid effects in RCMs, which contributes to over 50% of the total real-fluid effects on RCM autoignition reactivity.

Finally, to avoid misinterpretation of RCM autoignition experimental data and to eliminate the errors that have been and will be introduced into the simulation results obtained using the existing RCM modeling frameworks, we strongly suggest that future studies aiming to analyze and simulate past and new RCM experiments (particularly at high-pressure conditions) shall follow the approach proposed in the present study.

Acknowledgments

The work described in this paper is supported by the Research Grants Council of the Hong Kong Special Administrative Region, China under PolyU P0046985 for ECS project funded in 2023/24 Exercise, the Otto Poon Charitable Foundation under P0050998, the National Natural Science Foundation of China under 52406158, the Chief Executive's Policy Unit of HKSAR under the Public Policy Research Funding Scheme (2024.A6.252.24B), and the Natural Science Foundation of Guangdong Province under 2023A1515010976 and 2024A1515011486.

Declaration of Competing Interests

The authors declare no competing interests.

References

- [1] C.J. Sung, H.J. Curran, Using rapid compression machines for chemical kinetics studies, *Prog. Energy Combust. Sci* 44 (2014) 1-18.
- [2] S.S. Goldsborough, S. Hochgreb, G. Vanhove, M.S. Wooldridge, H.J. Curran, C.J. Sung, Advances in rapid compression machine studies of low-and intermediate-temperature autoignition phenomena, *Prog. Energy Combust. Sci* 63 (2017) 1-78.
- [3] S. Cheng, D. Kang, S.S. Goldsborough, C. Saggese, S.W. Wagnon, W.J. Pitz, Experimental and modeling study of C2–C4 alcohol autoignition at intermediate temperature conditions, *Prog. Energy Combust. Sci* 38 (2021) 709-717.
- [4] R.D. Büttgen, M. Preußker, D. Kang, S. Cheng, S.S. Goldsborough, G. Issayev, ... K.A. Heufer, Finding a common ground for RCM experiments. Part B: Benchmark study on ethanol ignition, *Combust. Flame* 262 (2024) 113338.
- [5] S.S. Goldsborough, S. Cheng, D. Kang, J.P. Molnar, Y.M. Wright, C.E. Frouzakis, Asynchronicity in opposed-piston RCMs: Does it matter? *Proc. Combust. Inst.* 40 (2024) 105406.
- [6] C.L. Barraza-Botet, S.W. Wagnon, & M.S. Wooldridge, Combustion chemistry of ethanol: ignition and speciation studies in a rapid compression facility, *J. Phys. Chem. A* 120 (2016) 7408-7418.
- [7] A. Ramalingam, Y. Fenard, A. Heufer, Ignition delay time and species measurement in a rapid compression machine: A case study on high-pressure oxidation of propane, *Combust. Flame* 211 (2020) 392-405.
- [8] S. Kang, W. Liao, Z. Chu, B. Yang, A rapid compression machine coupled with time-resolved molecular beam mass spectrometry for gas-phase kinetics studies, *Rev. Sci. Instrum* 92 (2021) 8.
- [9] A. Zdanowicz, J. Mohr, J. Tryner, K. Gustafson, B. Windom, D.B. Olsen, A.J. Marchese, End-gas autoignition fraction and flame propagation rate in laser-ignited primary reference fuel mixtures at elevated temperature and pressure, *Combust. Flame* 234 (2021) 111661.
- [10] R. Meier, *Methodological Developments for the Analysis of Biological Samples in the Presence of Compositional Effects*, 2020.
- [11] U. Retzer, H. Ulrich, S. Will, L. Zigan, Burst-mode 1-methylnaphthalene laser-induced fluorescence: Extended calibration and measurement of temperature and fuel partial density in a rapid compression machine, *Appl. Phys. B* 128 (2022) 144.
- [12] R. Dewor, C. Schulz, R.D. Büttgen, T. Brands, K.A. Heufer, H.J. Koß, Development of the first Raman scattering thermometry during the first stage ignition in a rapid compression machine and determination of detection limits for NO-LIF, *Appl. Energy Combust. Sci* 16 (2023) 100228.
- [13] E.F. Nasir, A. Farooq, Cavity-enhanced absorption sensor for carbon monoxide in a rapid compression machine, *Proc. Combust. Inst.* 37 (2019) 1297-1304.
- [14] K. Tanaka, S. Sugano, N. Yokota, S. Sakaida, M. Konno, H. Nakamura, Time-resolved mid-infrared measurements of hydrogen peroxide in the low-temperature oxidation of iso-octane in a rapid compression machine, *Combust. Sci. Technol* 194 (2022) 2042-2058.

- [15] C. Liu, H. Song, P. Zhang, Z. Wang, M.S. Wooldridge, X. He, G. Suo, A rapid compression machine study of autoignition, spark-ignition and flame propagation characteristics of H₂/CH₄/CO/air mixtures, *Combust. Flame* 188 (2018) 150-161.
- [16] S. Cheng, S.S. Goldsborough, S.W. Wagnon, W.J. Pitz, Probing intermediate temperature heat release in autoignition of C3-C4 iso-alcohol/gasoline blends, *Combust. Flame* 233 (2021) 111602.
- [17] S.S. Goldsborough, J. Santner, D. Kang, A. Fridlyand, T. Rockstroh, M.C. Jespersen, Heat release analysis for rapid compression machines: Challenges and opportunities, *Proc. Combust. Inst.* 37 (2019) 603-611.
- [18] J. Pan, Z. Zheng, H. Wei, M. Pan, G. Shu, X. Liang, An experimental investigation on pre-ignition phenomena: Emphasis on the role of turbulence, *Proc. Combust. Inst.* 38 (2021) 5801-5810.
- [19] R.D. Büttgen, M. Preußker, D. Kang, S. Cheng, S.S. Goldsborough, G. Issayev, K.A. Heufer, Finding a common ground for RCM experiments. Part B: Benchmark study on ethanol ignition, *Combust. Flame* 262 (2024) 113338.
- [20] H.T. Tizard, D.R. Pye, VIII. Experiments on the ignition of gases by sudden compression, *London Edinburgh Philos. Mag. & J. Sci* 44 (1922) 79-121.
- [21] H.T. Tizard, D.R. Pye, XCIX. Ignition of gases by sudden compression, *London Edinburgh Philos. Mag. & J. Sci* 1 (192)1094-1105.
- [22] G. Mittal, M.P. Raju, C.J. Sung, Computational fluid dynamics modeling of hydrogen ignition in a rapid compression machine, *Combust. Flame* 155 (2008) 417-428.
- [23] H. Hu, J. Keck, Autoignition of adiabatically compressed combustible gas mixtures, *SAE Trans*, 96 (1987) 592-604.
- [24] P. Park, J.C. Keck, Ignition delays for iso-octane: measurement using a rapid compression machine and prediction using a reduced chemical kinetic model, *SAE Tech. Pap* (1991) 912553.
- [25] P. Park, A.B. Mansfield, P.G. Arias, M.S. Wooldridge, H.G. Im, A computational study of syngas auto-ignition characteristics at high-pressure and low-temperature conditions with thermal inhomogeneities, *Combust. Theory Model* 19 (2015) 587-601.
- [26] A. Ramalingam, K. Zhang, A. Dhongde, L.H. Virnich, Sankhla, H. Curran, A. Heufer, An RCM experimental and modeling study on CH₄ and CH₄/C₂H₆ oxidation at pressures up to 160 bar, *Fuel* 206 (2017) 325-333.
- [27] S. Cheng, C. Saggese, D. Kang, S.S. Goldsborough, S.W. Wagnon, G. Kukkadapu, W.J. Pitz, Autoignition and preliminary heat release of gasoline surrogates and their blends with ethanol at engine-relevant conditions: Experiments and comprehensive kinetic modeling, *Combust. Flame* 228 (2021) 57-77.
- [28] S. Cheng, D. Kang, A. Fridlyand, S.S. Goldsborough, C. Saggese, S. Wagnon, D. Vuilleumier, Autoignition behavior of gasoline/ethanol blends at engine-relevant conditions, *Combust. Flame* 216 (2020) 369-384.
- [29] M. Wang, R. Tang, X. Ren, Y. Cui, S. Cheng, Ab initio intermolecular interactions mediate thermochemically real-fluid effects that affect system reactivity: The first application of high-order Virial EoS and first-principles multi-body potentials in trans-/super-critical autoignition modelling, *Combust. Flame* 272 (2025) 113844.

- [30] M. Wang, R. Tang, X. Ren, X. Ren, H. Wu, T. Zhang, S. Cheng, Investigation of real-fluid effects on NH₃ oxidation and blending characteristics at supercritical conditions via high-order Virial equation of state coupled with ab initio intermolecular potentials, *Combust. Flame* 272 (2025) 113887.
- [31] M.Wang, R. Tang, X. Ren, H. Wu, T. Zhang, S. Cheng, The first application of high-order Virial equation of state and ab initio multi-body potentials in modeling supercritical oxidation in jet-stirred reactors, *Fuel* 15 (2025) 382.
- [32] M.Wang, R. Tang, X. Ren, H. Wu, Y. Dong, T. Zhang, B. Yang, S. Cheng, Comprehensive Characterization of Real-Fluid Effects on Autoignition Behavior Via High-Order Virial Equation of State Coupled with Ab Initio Multi-Body Intermolecular Potentials, *SSRN* (2025) 5170386.
- [33] Y. Wu, S. Panigrahy, A.B. Sahu, C. Bariki, J. Beeckmann, J. Liang, H.J. Curran, Understanding the antagonistic effect of methanol as a component in surrogate fuel models: A case study of methanol/n-heptane mixtures, *Combust. Flame* 226 (2021) 229-242.
- [34] M.J. McNenly, R.A. Whitesides, D.L. Flowers, Faster solvers for large kinetic mechanisms using adaptive preconditioners, *Proc. Combust. Inst.* 35 (2015) 581-587.
- [35] A. Ramalingam, K. Zhang, A. Dhongde, L. Virnich, H. Sankhla, H. Curran, A. Heufer, An RCM experimental and modeling study on CH₄ and CH₄/C₂H₆ oxidation at pressures up to 160 bar, *Fuel*, 206 (2017) 325-333
- [36] B.W. Weber, C.J. Sung, M.W. Renfro, On the uncertainty of temperature estimation in a rapid compression machine, *Combust. Flame* 162 (2015) 2518-2528.